Applied Acoustics 70 (2009) 674–680

Contents lists available at ScienceDirect

Applied Acoustics

journal homepage: www.elsevier.com/locate/apacoust

Numerical prediction of tip vortex cavitation behavior and noise considering nuclei size and distribution

Kwangkun Park [a,1], Hanshin Seol [b,2], Wooyoung Choi [a,1], Soogab Lee [c,*]

[a] School of Mechanical and Aerospace Engineering, BD 313-118, Seoul National University, San56-1, Sillim-dong, Gwanak-gu, Seoul 151-742, Republic of Korea
[b] Maritime and Ocean Engineering Research Institute (MOERI), KORDI, Jang-Dong 171, P.O. Box 23, Yusung-Gu, Daejeon 305-343, Republic of Korea
[c] School of Mechanical and Aerospace Engineering, BD 311-105, Seoul National University, San56-1, Sillim-dong, Gwanak-gu, Seoul 151-742, Republic of Korea

ARTICLE INFO

Article history:
Received 12 October 2007
Received in revised form 9 July 2008
Accepted 7 August 2008
Available online 26 September 2008

Keywords:
Tip vortex cavitation
Hybrid method
Behavior
Noise
Nuclei

ABSTRACT

The tip vortex cavitation behavior and sound generation were numerically analyzed. A numerical scheme combining Eulerian flow field computation and Lagrangian particle trace approach was applied to simulate tip vortex cavitation. Flow field was computed by using hybrid method which combines Reynolds-Averaged Navier-Stokes solver with Dissipation Vortex Model. The trajectory and behavior of each cavitation bubble were computed by Newton's second law and Rayleigh–Plesset equation, respectively. According to nuclei population data, the cavitation nuclei were distributed and convected into the tip vortex flow. Calculated volume of the cavitation bubble and the trajectory were used as the input of cavitation bubble noise analysis. The relationship of cavitation inception, sound pressure level, and cavitation nuclei size was studied at several cavitation numbers. It was found that cavitation inception of smaller nuclei is more sensitive to the change of cavitation number and cavitation noise due to the cavitated smallest nuclei has the most influence on overall tip vortex cavitation noise.

1. Introduction

Cavitation reduces the mechanical efficiency and causes vibration, noise and erosion [1]. Especially, "cavitation noise generated by a propeller is critical in underwater detection, and is often related to the survivability of the vessels especially for military purposes. Cavitation of the marine propeller is the most prevalent source of underwater sound in oceans and is often the dominant noise source of a marine vehicle" [2]. There are various types of cavitation for example, tip vortex cavitation, sheet cavitation, bubble cavitation, cloud cavitation. Each cavitation type has a different formation mechanism. The tip vortex cavitation is produced by low pressure in a tip vortex field, and it is the first type of cavitation to appear with intense noise. Therefore, to design the low noise propeller and hydrofoil, it is necessary to understand the generation mechanism, behavior and noise of tip vortex cavitation.

Several methods have been used by previous researchers to simulate cavitation flow numerically, for example, inter-phase tracking method, continuum method, and Rayleigh–Plesset equation based method. Among these methods, Rayleigh–Plesset equation based method is the most proper to predict the cavitation noise, because volume variation data of cavitation bubble can be obtained. Using Rayleigh–Plesset equation, analysis of cavitation bubble has been studied by many researchers. The collapse of a single spherical bubble in the unbounded liquid was first treated by Rayleigh [3]. Later it was supplemented by Plesset [4]. Kubota et al. [5] described the behavior of the cavitation bubble. Shen et al. [6], Hsiao and Chahine [7] also studied the cavitation bubble dynamics in tip vortex cavitation.

In this study, Eulerian–Lagrangian approach is applied to predict tip vortex cavitation behavior and noise based on the Rayleigh–Plesset equation. In this approach, carrier flow of cavitation bubble is computed by Eulerian and cavitation bubble is analyzed by Lagrangian [8]. It is one-way coupled method, and it is assumed that presence of cavitation bubbles in the flow does not significantly alter carrier flow. This assumption is reasonable since cavitation bubbles are so small that the mass, momentum and energy of bubbles give little influence on flow field [8].

Reynolds-Averaged Navier-Stokes solver (RANS, hereinafter)/Dissipation Vortex Model (DVM, hereinafter) hybrid method is applied for the efficient Eulerian flow field analysis. The flow field result of RANS solver is used for obtaining the initial conditions for vortex modeling. Bubble dynamics is computed by the numerical modeling of Rayleigh–Plesset equation, which is coupled with nuclei trajectory equation. Cavitation nuclei distribution data [9] is converted to computational nuclei population. According to the population data, the nuclei are distributed and released in the tip vortex flow field, and then they are analyzed by Lagrangian ap-

* Corresponding author. Tel.: +82 2 880 7384; fax: +82 2 875 4360.
E-mail addresses: pkk78@snu.ac.kr (K. Park), hsseol@moeri.re.kr (H. Seol), yanni1@snu.ac.kr (W. Choi), solee@snu.ac.kr (S. Lee).
[1] Tel.: +82 2 880 7384.
[2] Tel: +82 42 868 7695.

0003-682X/$ - see front matter © 2008 Elsevier Ltd. All rights reserved.
doi:10.1016/j.apacoust.2008.08.003

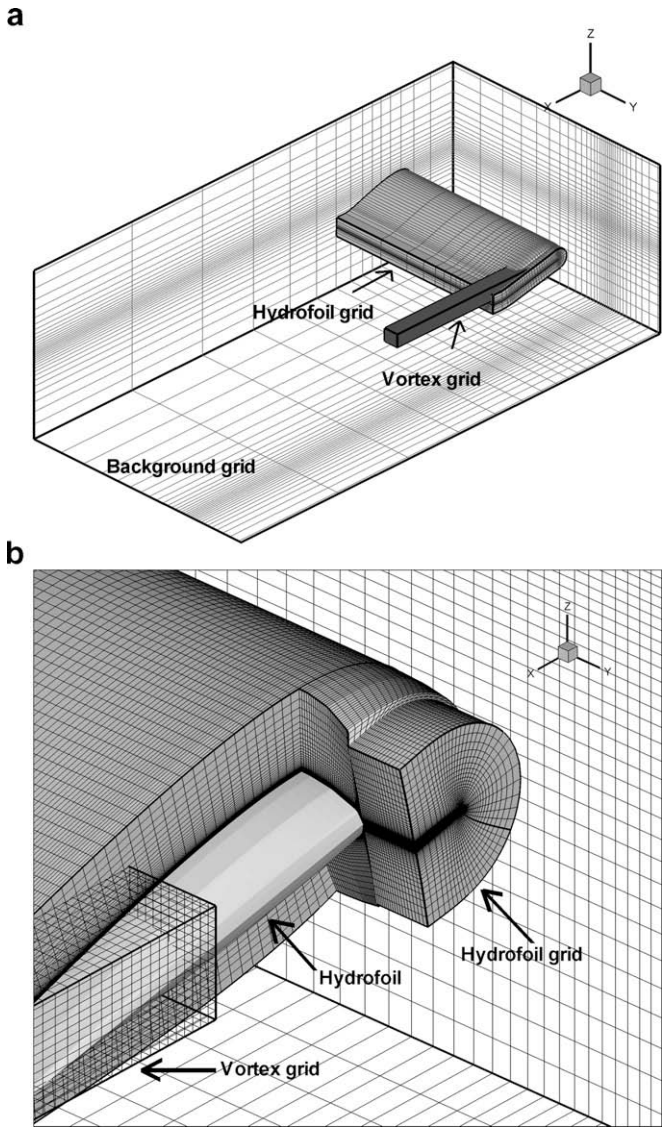

Fig. 1. Chimera grid system of model hydrofoil for RANS calculation: (a) whole grid, and (b) detailed view in the tip region.

proach. Using these numerical methods, cavitation bubble trajectory and behavior are computed for the nuclei with each different initial size.

Through this study, the behavior and noise results of tip vortex cavitation are presented on cavitation nuclei size, and they help understand tip vortex cavitation generation mechanism and its noise characteristics.

2. Methodology

In order to analyze the tip vortex cavitation behavior and noise, Eulerian flow field analysis is performed prior to Lagrangian one. Bubble trajectory based on the Newton's second law and the Rayleigh–Plesset equations are solved for each nucleus, which is distributed and released in the computational flow field. The nuclei trajectories are calculated considering various acting forces on the nuclei. Calculated radius variation of the cavitation bubble and the trajectory are used as the input of cavitation bubble noise analysis.

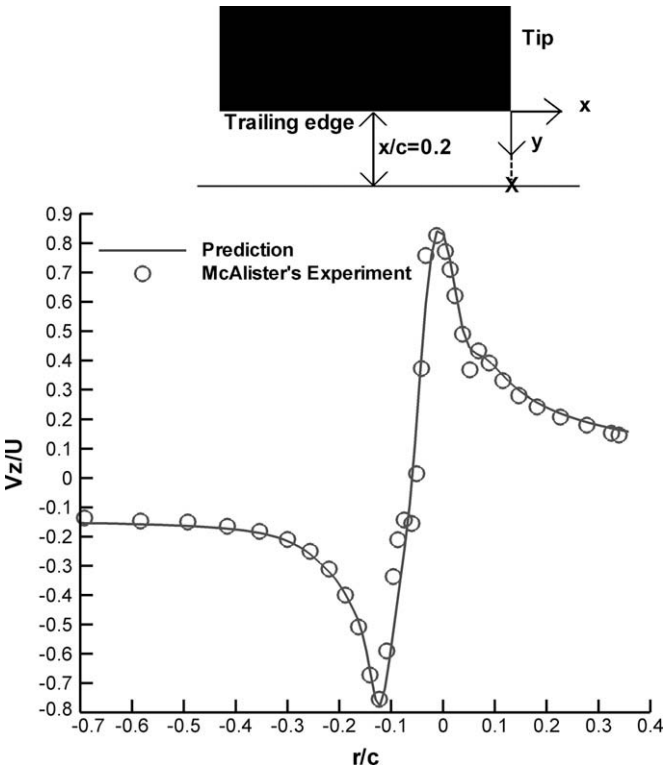

Fig. 2. Vertical velocity across the tip vortex at $x/c = 0.2$, (NACA0015 section, AOA = 12°, $Re = 1.5 \times 10^6$) [20].

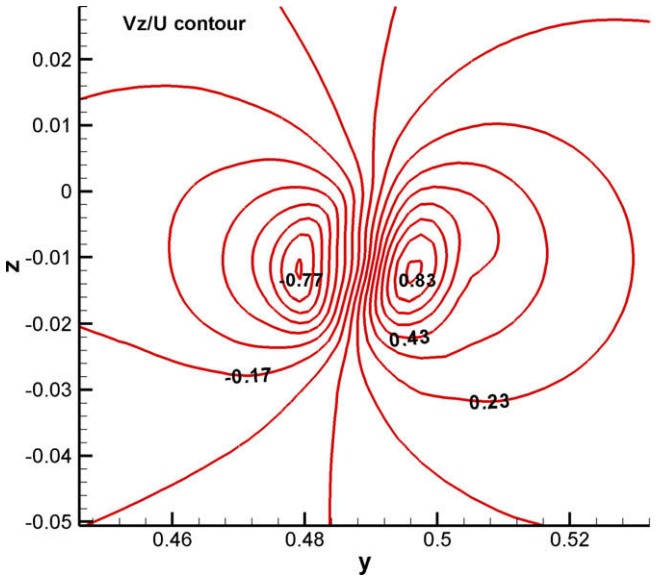

Fig. 3. Non-dimensional vertical velocity contour for the initial value of vortex model, difference value between contour lines, $\Delta \frac{Vz}{U_\infty} = 0.01$.

2.1. Flow solver

For the analysis of the tip vortex cavitation behavior and noise, Eulerian flow field analysis is prior to Lagrangian one. The tip vortex flow is obtained by using the Scully vortex model [10,11], because general Computational Fluid Dynamics (CFD, hereinafter) technique requires massive grid points and large amount of computational time to capture the tip vortex. Furthermore, common CFD technique can capture tip vortex only $2 \sim 5$ times chord length of hydrofoil due to numerical dissipation.

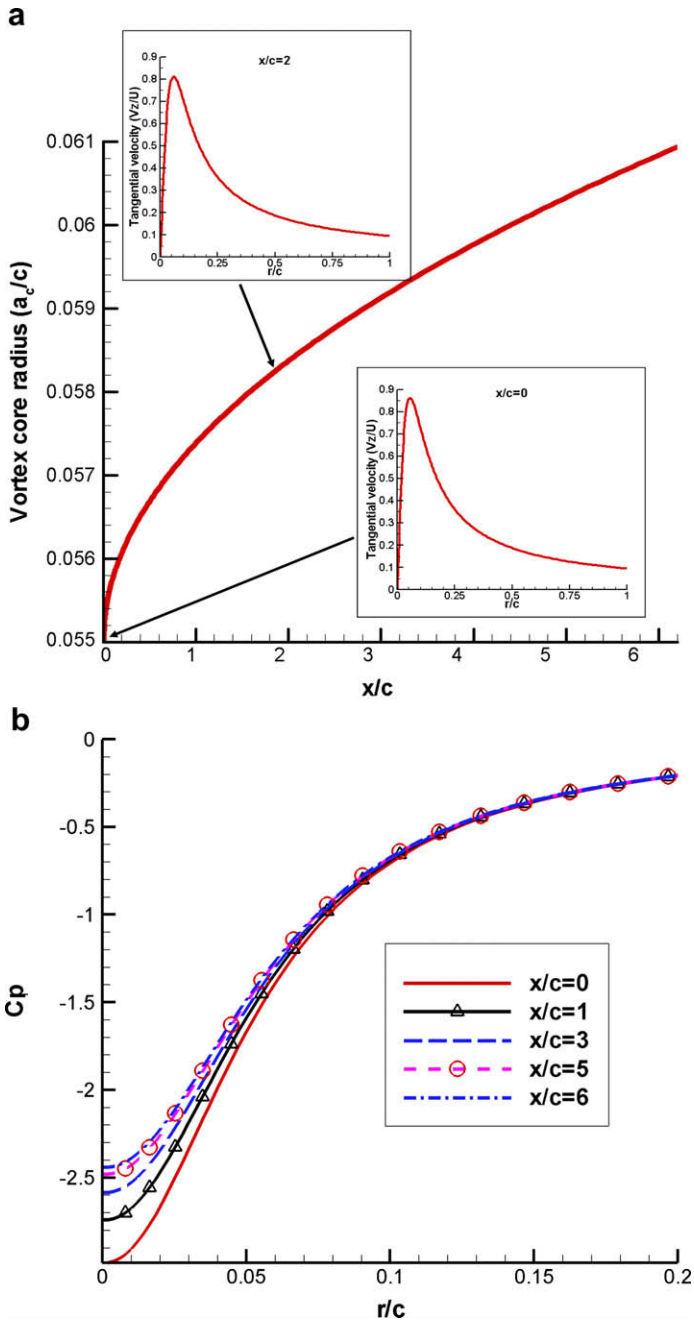

Fig. 4. Tip vortex flow field for Eulerian approach: (a) vortex core radius variation with respect to distance from trailing edge and tangential velocity distribution, and (b) pressure coefficient across the tip vortex core.

The Scully vortex model is expressed as follows.

$$V_\theta = \frac{\Gamma}{2\pi}\frac{r}{r^2 + a_c^2} \qquad (1)$$

$$\Gamma = \frac{\Gamma_\infty}{r^2 + a_c^2}$$

V_θ, a_c, and Γ_∞ are tangential velocity, vortex core radius and total circulation, respectively. The Scully vortex model is two dimensional model that can not consider the change of vortex core radius in the downstream direction. The tip vortex is weakened and vortex core is expanded due to dissipation as the tip vortex moves downstream in real phenomena. Therefore in order to simulate the tip vortex flow more accurately, the vortex core radius variation modeling is required. Moore and Saffman [12] predicted the tip vortex core radius variation by assuming the viscous dissipation. The equation from Moore and Saffman is as follows.

$$r^* = \frac{a_c Re_c^{1/2}}{c} = 2.92\left(\frac{x}{c}\right)^{1/2} \qquad (2)$$

Here, r^* denotes dimensionless vortex core radius. Re_c and a_c are chord based Reynolds number and the vortex core radius, respectively. Eq. (2) is grafted to Eq. (1) to consider the vortex core radius variation in downstream direction. To calculate Eq. (1), initial values (vortex core radius, total circulation and tangential velocity) are needed. Such initial values can be acquired by solving the unsteady RANS equation.

It uses an implicit finite volume method and Baldwin–Lomax turbulence modeling. Implicit finite volume method is used for

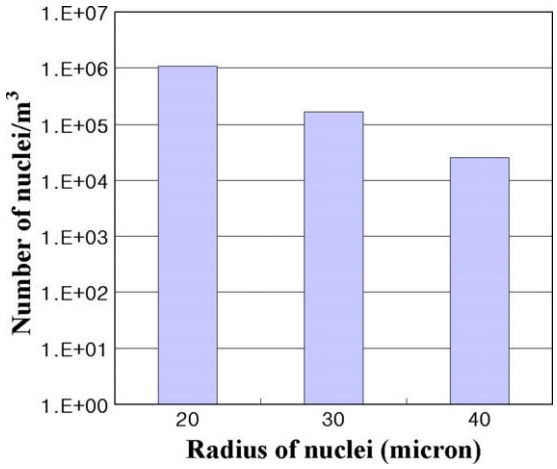

Fig. 5. Cavitation nuclei population data at sea water [9].

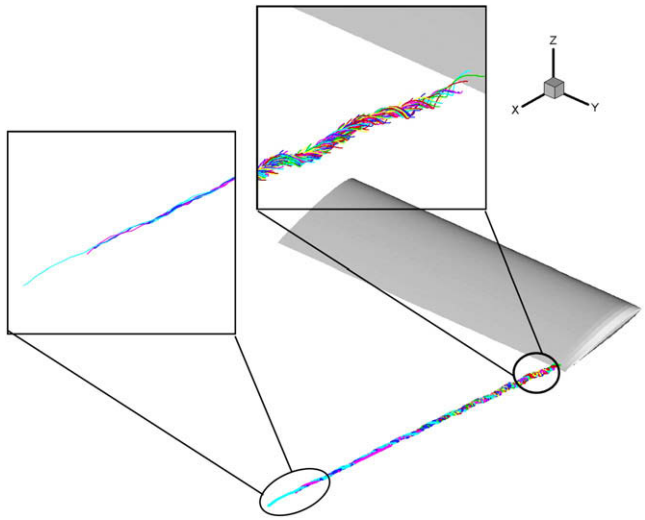

Fig. 7. Trajectories of cavitating nuclei. (σ = 2.45).

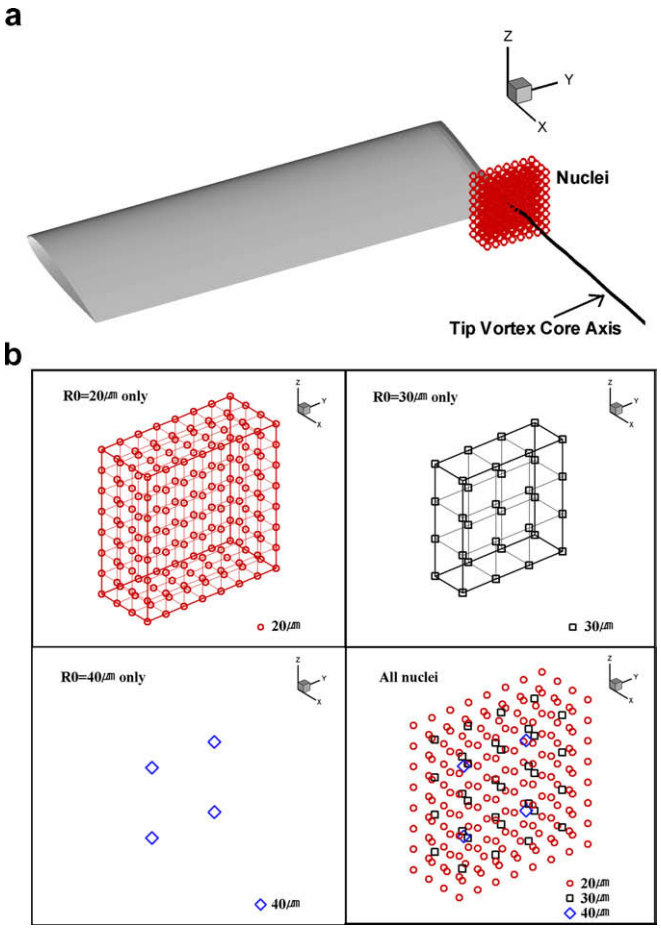

Fig. 6. Initial nuclei distribution in the tip vortex flow field: (a) bird's eye-view, and (b) enlarged view.

solving this equation in general time dependent curvilinear coordinate system. The convective terms are discretized using Roe's flux difference splitting method combined with the Weighted Essentially Non-Oscillatory, and Lower-Upper Symmetric Gauss-Seidel (LU-SGS) method is adopted to perform time numerical integration [13–15].

To capture tip vortex accurately in the tip region, an overset grid system is used. The grid system is composed of one C–H type hydrofoil grid, H–H type tip vortex grid, and H–H type background grid (Fig. 1). The C–H grid on the hydrofoil contains 149 × 124 × 49 grid points in the chordwise, spanwise and normal direction. The background grid and vortex grid contain 126 × 126 × 61 and 151 × 126 × 51 grid points in the spanwise direction, the normal direction and the streamwise direction, respectively. To predict the tip vortex cavitation on a hydrofoil, rectangular planform with NACA0015 section hydrofoil is used.

2.2. Numerical modeling of bubble dynamics and noise analysis method

The dynamics of bubbles in a liquid responding to an imposed pressure fluctuation has been considered. The Rayleigh–Plesset equation is derived from the continuity and momentum equations, describes the dynamics of spherical bubbles in a variable pressure field. In this study, modified Rayleigh–Plesset equation which slip velocity is added to Rayleigh–Plesset equation is used. It takes the form [6]:

$$R\ddot{R}+\frac{3}{2}\dot{R}^2=\frac{1}{\rho}\left(p_v+p_{g_0}\left(\frac{R_0}{R}\right)^{3k}-p-\frac{2\gamma}{R}-\frac{4\mu}{R}\dot{R}\right)+\frac{(\vec{U}-\vec{U}_b)^2}{4} \quad (3)$$

where R is the radius of the bubble, $\vec{U}$ is the velocity, p_v is the vapor pressure, p_g is the gas pressure, γ is the surface tension, μ is the viscosity, and subscript b indicates property of the bubble.

Eq. (3) is a second order nonlinear ordinary differential equation. To solve this nonlinear equation, it is required that the second order differential equation is changed into the coupled set of first order differential equations, and the fourth order Runge-Kutta method is applied to solve these equations [16].

Many studies have been devoted to analyze the motions of particle and bubbles. The study of Maxey and Riley [17] is well described the actual motion of the rigid spherical particles, which are subjected to the various forces. Spherical bubble motion can be written as follows [6,17].

$$\rho_b\tfrac{4}{3}\pi R^3\tfrac{d\vec{U}_b}{dt}=\tfrac{4}{3}\pi R^3(\rho_b-\rho)\vec{g}-\tfrac{4}{3}\pi R^3\nabla p+\tfrac{1}{2}\rho\pi R^2C_D(\vec{U}-\vec{U}_b)|\vec{U}-\vec{U}_b|+\tfrac{1}{2}\tfrac{4}{3}\pi R^3\rho\left(\tfrac{d\vec{U}}{dt}-\tfrac{d\vec{U}_b}{dt}\right)+6\pi R^2\sqrt{\tfrac{\rho\mu}{\pi}}\int_0^t\frac{\frac{d\vec{U}}{d\tau}-\frac{d\vec{U}_b}{d\tau}}{\sqrt{t-\tau}}d\tau \quad (4)$$

As terms in the right hand side of Eq. (4) mean forces on the bubble, each term respectively represents the buoyancy force, pressure gradient, drag force, force due to added mass, and Basset term which

Table 1
Number of cavitated nuclei and sound pressure level on cavitation number and nuclei size (N_{Cav}: number of cavitated nuclei, N_{Total}: number of total nuclei)

Cavitation number	$R0$ = 20 μm		$R0$ = 30 μm		$R0$ = 40 μm		Overall SPL(dB)
	$\frac{N_{Cav.}}{N_{Total}}$	SPL(dB)	$\frac{N_{Cav.}}{N_{Total}}$	SPL(dB)	$\frac{N_{Cav.}}{N_{Total}}$	SPL(dB)	
2.58	250/256	151	32/32	143	4/4	131	152
2.60	250/256	149	32/32	142	4/4	130	150
2.62	247/256	148	32/32	138	4/4	129	149
2.64	244/256	146	32/32	138	4/4	128	147
2.66	213/256	144	32/32	136	4/4	125	144
2.68	162/256	143	26/32	133	4/4	124	143
2.70	117/256	140	22/32	132	3/4	120	141
2.72	66/256	137	14/32	129	2/4	118	137

Table 2
Critical pressure on cavitation number and nuclei size (unit: Pa)

Cavitation number	$R0$ = 20 μm	$R0$ = 30 μm	$R0$ = 40 μm
2.58	933	1509	1769
2.60	936	1511	1770
2.62	939	1513	1771
2.64	942	1515	1773
2.66	945	1517	1774
2.68	949	1518	1775
2.70	951	1520	1776
2.72	955	1522	1778

denotes memory effect. Pressure gradient is computed by the pressure difference between the bubble walls. Buoyancy and drag force terms are computed along the bubble radius variations. The drag coefficient and bubble Reynolds number are calculated by the Harberman's empirical formulation [18]. The bubble Reynolds number is based on the velocity difference due to slip between the bubble and the liquid.

$$\frac{C_D Re_b}{24} = 1.0 + 0.197 Re_b^{0.63} + 2.6 \times 10^{-4} Re_b^{1.38} \tag{5}$$

$$Re_b = \frac{2R|\vec{U} - \vec{U}_b|}{\nu} \tag{6}$$

Rayleigh–Plesset equation and the equation of motion are solved sequentially in the time step. The bubble size is calculated through Eq. (3), and the motion of the bubble is computed by using updated radius of the bubble in Eq. (4). In the next time step, the velocity of the bubble and pressure on the bubble are used to calculate Eq. (3).

Cavitation noise is very difficult to predict exactly through theoretical and numerical methods. However the single bubble noise theory provides a basis for scaling experimentally measured sounds [19]. It is also the basis of modern theoretical modeling of the hydrodynamic tip vortex cavitation noise [19]. In the theory, cavitation bubbles behave as monopole sources. The acoustic pressure in the far field due to the bubble is given as follows.

$$p'(t) = \frac{\rho_0 \ddot{V}_b\left(t - \frac{r}{c}\right)}{4\pi r|1 - M_r|} \tag{7}$$

Since the bubble volume is $V_b = (4/3)\pi R^3$, and the second time derivative of the volume is $\ddot{V}_b = 4\pi R(2\dot{R} + R\ddot{R})$. M_r is relative Mach number and means Mach number of the radiation direction. The term $t - r/c$ is the retarded time.

3. Results and discussion

In this section, the tip vortex flow field, bubble trajectory and dynamics results are presented. The noise characteristic is analyzed by using these data. Based on the condition of the undisturbed medium of standard sea water, the density and the speed of sound are chosen as 1026 kg/m^3 and 1500 m/s, respectively. Calculated three dimensional hydrofoil is rectangular with an aspect ratio of 6.6 and has NACA0015 section with the chord length of c = 0.15 m. The simulation is implemented for chord based Reynolds number, of $Re = 1.5 \times 10^6$ and angle of attack of 12°. Using the local conditions along the nucleus trajectory, the instantaneous pressure is calculated. When the pressure on the nucleus is lower than the critical pressure of each nucleus, the nucleus starts to grow into the cavitation bubble. Tip vortex cavitation behavior and noise are predicted at several cavitation numbers. Cavitation number is defined as below.

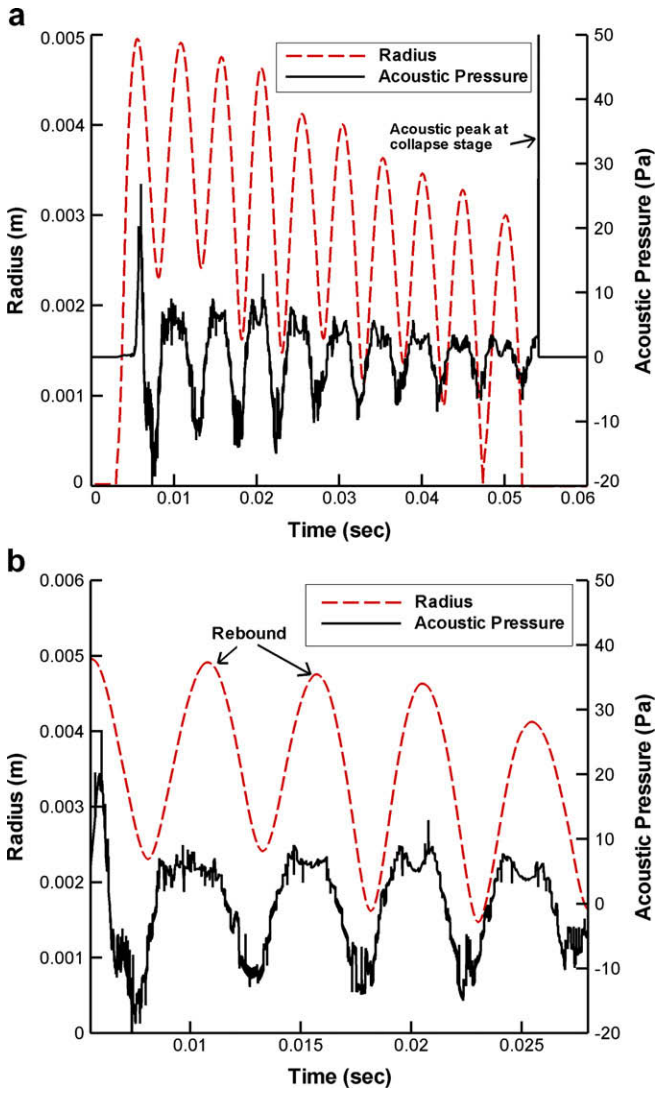

Fig. 8. Relationship between bubble radius variation and acoustic pressure: (a) whole time domain and (b) detailed view.

$$\sigma = \frac{p_\infty - p_v}{\frac{1}{2}\rho_\infty U_\infty^2} \quad (8)$$

The noise analysis is performed at the observer position of (0, 20*c*, 0). The origin is located in the trailing edge of the hydrofoil tip. Reference pressure for the sound pressure level is 1 μPa. Initial vortex core radius and total circulation are needed to calculate Eulerian flow field using DVM, and these values are obtained from CFD result. To validate CFD program used in this study, the result of vertical velocity across the tip vortex is shown in Fig. 2. Predicted vertical velocity and the vortex core radius are in good agreement with experimental result [20].

Fig. 3 displays the vertical velocity distribution at just behind of trailing edge of the hydrofoil. Free stream velocity based dimensionless maximum tangential velocity is 0.86, and initial core radius is 0.055*c*. Calculated initial vortex core radius and total circulation are used as the input of vortex modeling. Generally, vortex core axis is considered to be located on the lowest pressure point, and the vortex core radius is equal to the distance between the vortex core axis and a point with maximum tangential velocity. Therefore, vortex core trajectory can be found by tracing the minimum pressure region of tip vortex flow. The total circulation is deduced from the known vortex core radius and maximum tangential velocity in Eq. (1) [21].

Results of Eulerian flow field computed by RANS and DVM hybrid method are shown in Fig. 4. They display tangential velocity profile behind the trailing edge, vortex core radius variation (Fig. 4a) and pressure coefficient across the tip vortex core (Fig. 4b), respectively. The vortex core radius and pressure are increased, as the vortex moves downstream.

A liquid contains a lot of nuclei, and the pressure of the nuclei balances with the surface tension. The size of nuclei generally ranges from 1 μm to hundreds μm. To consider nuclei in the sea water, nuclei population data is obtained from O'Hern's cavitation nuclei number density distribution function [9]. Nuclei population data are converted to computational nuclei population which represents distributed number per unit volume (Fig. 5). The nuclei are distributed near the tip vortex core region of the trailing edge as shown in Fig. 6a. Virtual volume of distributed nuclei is equal to 0.08 m × 0.08 m × 0.04 m in the *y*, *z*, and *x* directions. According to the O' Hern's nuclei population data, the nuclei with radius 20 μm, 30 μm, and 40 μm are simulated. The numbers of nuclei with radius of 20 μm, 30 μm, 40 μm are 256, 32, 4, respectively (Fig. 6b). Each nucleus which is released in the flow field is traced from Lagrangian particle trace method.

Fig. 7 shows nuclei trajectories while the nuclei cavitate. The bubbles show helical motion and move inboard of the hydrofoil span as going downstream, according to characteristics of the tip vortex flow. Generally, visual method and acoustic method are used for the estimation criterion of cavitation occurrence. In this study, we consider that cavitation event is occurred when the radius of nuclei is larger than 0.001 m. Cavitation bubbles are appeared more in the trailing edge region than in the downstream region away from the trailing edge. It is due to wide low pressure region close to trailing edge.

Changing the cavitation number, the number of cavitated nuclei is shown in Table 1. It shows that the numbers of cavitated nuclei decrease, as the cavitation number increases. However, the decreasing rate of the number of cavitated nuclei is different as the nuclei size. Among them, the smallest nuclei show the highest decreasing rate in most range. The critical pressure is increased by 3 or 4 Pa, as the cavitation number is increased by 0.02, in the nuclei with the initial radius of 20 μm (Table 2). On the other hand, the increase of critical pressure is about 1 Pa, for nuclei with the initial radius of 40 μm. It shows that the critical pressure change of small nuclei is bigger than that of large nuclei with the change

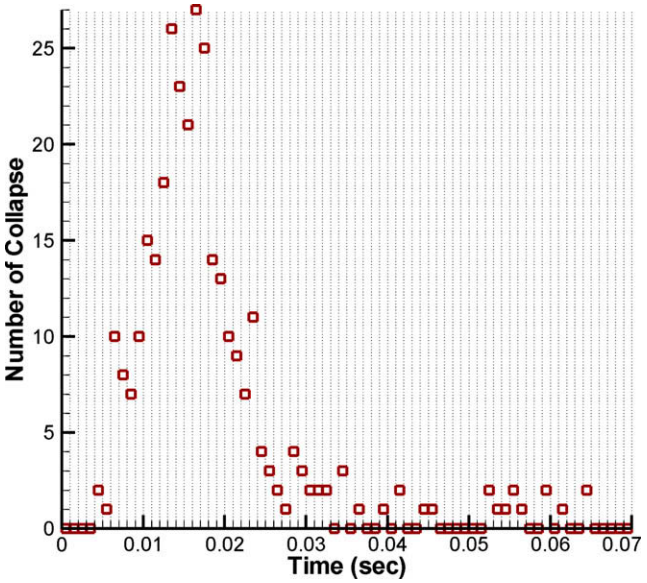

Fig. 9. Accumulation number of collapse in the 0.001 s time bandwidth. (σ = 2.45).

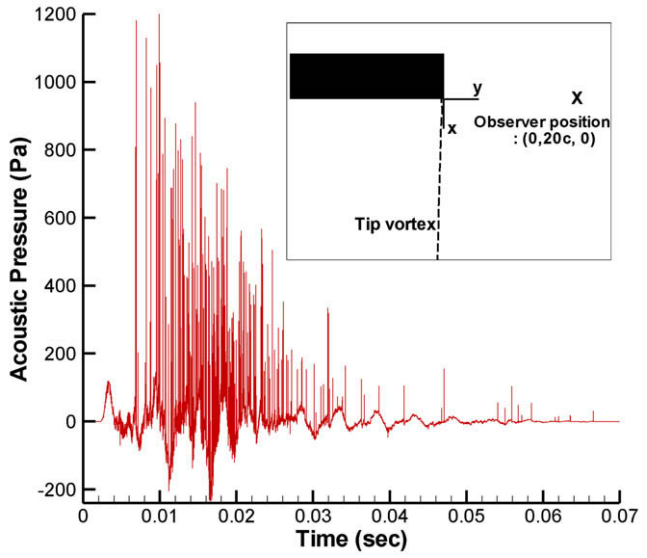

Fig. 10. Computation result of acoustic pressure of cavitation bubbles. (σ = 2.45).

of cavitation number. It can be deduced that cavitation inception of small nuclei is more sensitive to the change of cavitation number than that of large nuclei.

As the cavitation number changes from 2.58 to 2.72, the decrease of the sound level on each nuclei size is almost same. Comparing sound pressure levels at each nuclei size, the most intensive sound is generated by nuclei of initial radius of 20 μm. The overall sound level is the same level as sound of nuclei of 20 μm or is slightly higher than sound level of nuclei of 20 μm. Although small nuclei have less chance to cavitate due to low critical pressure, the small cavitated nuclei are more abundant than larger nuclei. It shows that noise due to cavitated smallest cavitation nuclei has the most influence on the overall sound pressure level of tip vortex cavitation noise.

Fig. 8 displays relationship between bubble radius variation and acoustic pressure. The cavitation bubble shown in Fig. 8 is chosen arbitrarily among the bubbles with radius of 20 μm at cavitation

number, $\sigma = 2.45$. Several rebounds are observed. As the rebound proceeds, the growth of bubble radius decreases as shown in Fig. 8a. It is because rebound radius decreases due to the pressure increase in the vortex core region as the tip vortex moves downstream. The cavitation noise is proportioned to the second time derivative of bubble volume. Therefore, the acoustic peak is occurred at around 0.055 s when the bubble collapses rapidly. In the noise prediction, there is a time difference of about 0.002 s between cavitation behavior and acoustic signal, because the distance between observation point and cavitation occurrence position is about 20*c*.

Fig. 8b shows rebound behavior and noise in detail. Considering the time difference, the growth of the radius results in increasing acoustic pressure and decrease of the radius leads to decreasing acoustic pressure. Fig. 9 represents the accumulation number of collapse of the bubbles in each 0.001 s time band width. For instance, at between 0.006 s and 0.007 s, collapses occur 10 times, and then they result in noise peaks at about 0.009 s due to a time delay. Comparing Fig. 9– 10, it is shown that the collapses at between 0.006 s and 0.03 s result in many noise peaks.

4. Concluding remarks

In this study, tip vortex cavitation behavior and noise are numerically analyzed by Eulerian–Lagrangian approach. For the analysis of behavior and noise, tip vortex flow analysis is preceded. RANS and DVM hybrid method is used to obtain Eulerian vortex flow field with saving computation time and has strong point in aspect of considering the dissipation of the tip vortex compared to other vortex models. Bubble behavior is predicted by modified Rayleigh–Plesset equation, which is coupled with nuclei trajectory equation. For the simulation of nuclei in the sea water, O'Hern's experimental nuclei population data is converted to the computational nuclei population. The tip vortex cavitation noise is predicted based on the bubble trajectory and volume variation results. As the cavitation noise is proportioned to the second time derivative of bubble volume, strong sound is emitted at the collapse stage. The relationship of cavitation inception, sound pressure level, and cavitation nuclei size was studied at several cavitation numbers. This study shows that cavitation inception of smaller nuclei is more sensitive to the change of cavitation number. Cavitation noise level due to cavitated smallest nuclei has the most influence on overall tip vortex cavitation noise. It is expected that slight weakening of tip vortex could largely reduce the noise due to tip vortex cavitation.

Acknowledgement

This work is outcome of the fostering project of the Best Lab supported financially by the Ministry of Commerce, Industry and Energy (MOCIE) in Korea. This work was supported by Defense Acquisition Program Administration and Agency for Defense Development under the contract UD070041AD.

References

[1] Weitendorf EA. Cavitation phenomena, propeller excited hull pressure amplitudes and cavitation scale effect. Ocean Eng 1981;8(5):517–39.
[2] Seol H, Suh J, Lee S. Development of hybrid method for the prediction of underwater propeller noise. J Sound Vibr 2005;288:345–60.
[3] Rayleigh L. On the pressure development in a liquid during the collapse of a spherical cavity. Philos Mag 1917;34:94–8.
[4] Plesset MS. Dynamics of cavitation bubbles. J Appl Mech 1948;16:228–31.
[5] Kubota A, Kato H, Yamaguchi H. A new modeling of cavitating flows: a numerical study of unsteady cavitation on a hydrofoil section. J Fluids Mech 1992;240:59–96.
[6] Shen Y, Chahine GL, Hsiao CT, Jessup SD. Effect of model size and free stream nuclei on tip vortex cavitation inception scaling. In: Fourth international symposium on cavitation, Pasadena, CA, USA; 2001.
[7] Hsiao CT, Chahine GL. Prediction of vortex cavitation inception using coupled spherical and non-spherical models and UNRANS computations. In: 24th symposium on naval hydrodynamics, Fukuoka, Japan; 2002.
[8] Farrell KJ. Eulerian/Lagrangian analysis for the prediction of cavitation inception. In: Fourth international symposium on cavitation, Institute of Technology, Pasadena, CA, USA; 2001.
[9] O'Hern T, d'Agostino L, Acosta AJ. Comparison of holographic and Coulter counter measurements of cavitation nuclei in the ocean. ASME J Fluids Eng 1988;110:200–7.
[10] Scully MP. Computational of Helicopter rotor wake geometry and its influence on rotor harmonic loads. ASRL TR-178-1 MIT 1975.
[11] Hinton DA, Tatnall CR. A candidate wake vortex strength definition for application to the NASA aircraft vortex spacing system. NASA Technical Memorandum 1997:110343.
[12] Moore DW, Saffman PG. Axial flow in laminar trailing vortices. Proc Roy Soc Lond A 1973;333:491–508.
[13] Roe PL. Approximate Riemann solvers, parameter vectors, and difference schemes. J Comput Phys 1981;43:357–72.
[14] Jiang G, Shu CW. Efficient implementation of weighted ENO schemes. J Comput Phys 1996;126:202–28.
[15] Yoon SK, Kwak DC. Three-dimensional incompressible Navier-Stokes solver using lower-upper symmetric-Gauss-Seidel algorithm. AIAA J 1991;29:874–5.
[16] Ligneul P, Latorre R. Study on the capture and noise of spherical nuclei. Acoustica 1989;68:1–14.
[17] Maxey MR, Riley JJ. Equation of motion for a small rigid sphere in a non-uniform flow. Phys Fluids 1983;26(4):883–9.
[18] Haberman WL, Morton RK. An experimental investigation of drag and shape of air bubbles rising in various liquids. DTMB Report 1953:802.
[19] Blake WK. Mechanics of flow-induced sound and vibration. Orlando: Academic Press Inc.; 1986.
[20] McAlister KW, Takahashi RK. NACA0015 Wing pressure and trailing vortex measurements. NASA Technical Paper 3151; 1991.
[21] Turner GP, Padfield GD, Harris M. Encounters with aircraft vortex wakes: the impact on helicopter handling qualities. J Aircraft 2002;39(5):839–49.